Spatial and phasic oscillation of non-Newtonian wall shear stress in human left coronary artery bifurcation: an insight to atherogenesis

Johannes V. Soulis[a], George D. Giannoglou[b], Yiannis S. Chatzizisis[b], Thomas M. Farmakis[b], George A. Giannakoulas[b], George E. Parcharidis[b] and George E. Louridas[b]

Objective **To investigate the wall shear stress oscillation in a normal human left coronary artery bifurcation computational model by applying non-Newtonian blood properties and phasic flow.**

Methods **The three-dimensional geometry of the investigated model included the left main coronary artery along with its two main branches, namely the left anterior descending and the left circumflex artery. For the computational analyses a pulsatile non-Newtonian flow was applied. To evaluate the cyclic variations in wall shear stress, six characteristic time-points of the cardiac cycle were selected. The non-Newtonian wall shear stress variation was compared with the Newtonian one.**

Results **The wall shear stress varied remarkably in time and space. The flow divider region encountered higher wall shear stress values than the lateral walls throughout the entire cardiac cycle. The wall shear stress exhibited remarkably lower and oscillatory values in systole as compared with that in diastole in the entire bifurcation region, especially in the lateral walls. Although the Newtonian wall shear stress experienced consistently lower values throughout the entire cardiac cycle than the non-Newtonian wall shear stress, the general pattern of lower wall shear stress values at the lateral walls, particularly during systole, was evident regardless of the blood properties.**

Conclusions **The lateral walls of the bifurcation, where low and oscillating wall shear stress is observed, are more susceptible to atherosclerosis. The systolic period, rather than the diastolic one, favors the development and progression of atherosclerosis. The blood viscosity properties do not seem to qualitatively affect the spatial and temporal distribution of the wall shear stress.** ***Coron Artery Dis*** **17:351–358 © 2006 Lippincott Williams & Wilkins.**

Coronary Artery Disease 2006, **17**:351–358

Keywords: computational analysis, coronary atherosclerosis, non Newtonian blood, phasic flow, wall shear stress

[a]Fluid Mechanics Division, School of Engineering, Democrition University of Thrace, Xanthi and [b]Cardiovascular Engineering and Atherosclerosis Laboratory, First Cardiology Department, AHEPA University Hospital, Medical School, Aristotle University of Thessaloniki, Thessaloniki, Greece

Correspondence and request for reprints to George D. Giannoglou, MD, PhD, Cardiovascular Engineering and Atherosclerosis Laboratory, First Cardiology Department, AHEPA University Hospital, Medical School, Aristotle University of Thessaloniki, 1 St. Kyriakidi Street, 54636 Thessaloniki, Greece
Tel/fax: +30 2310 994837; e-mail: yan@med.auth.gr

Sponsorship: A grant from the Greek State Scholarships Foundation.

Received 22 September 2005 **Accepted** 10 January 2006

Introduction

Today, a large body of evidence supports the fact that, apart from the systemic risk factors, biomechanical parameters are also involved in the initiation and proliferation of coronary atherosclerosis [1]. The involvement of these parameters could possibly explain the preferential localization of atherosclerosis at certain regions of the coronary arteries, despite the fact that all coronary segments are equally exposed to the deleterious effects of systemic risk factors [2]. Among the local biomechanical factors, wall shear stress (WSS) has been proven to be the most decisive one; however, its specific pathophysiological implication in atherogenesis is still under investigation. According to clinical observation, regions where disturbed flow occurs (e.g. bifurcations, branches, curves) have been shown to be more prone to atherosclerosis [1,3–5]. It is in these complex regions that blood velocity and WSS mainly exhibit low values or oscillate in both magnitude and direction over short distances. In recent years, the use of computational fluid dynamics (CFD) rules to solve the governing Navier–Stokes flow equations has become reasonably practical and reliable. The distribution of local hemodynamic parameters can be analyzed through the application of CFD in human coronary arteries in order to elucidate their possible contribution to atherogenesis.

Besides the spatial distribution of flow parameters, which have already been studied extensively, their temporal variation during the cardiac cycle has also been proposed

0954-6928

as a decisive atherogenic factor. The atherogenic impact of the temporal variation, however, has not been adequately investigated [2,5,6]. In the great majority of previous computational studies, the coronary flow was considered as steady; that is, a constant flow velocity was applied, although the flow throughout the arterial tree is pulsatile by nature [2,7]. The application of unsteady flow constitutes a challenging issue, as it demands manifold computational power and analysis time. Numerical studies of pulsatile flow through arterial stenosis, with emphasis on WSS effects, were carried out by Tu *et al.* [8]. In another study, He and Ku [9] performed computational analysis in a left coronary artery (LCA) bifurcation model and concluded that low and oscillatory WSS correlates strongly with the localization of atherosclerosis. Similar studies were conducted in three-dimensional (3D) carotid bifurcation models, investigating the flow phenomena under different bifurcation angles [10,11]. Nevertheless, in all the aforementioned studies, blood was treated as a Newtonian fluid, although physiologically it is characterized by non-Newtonian properties. Until now, very few studies have been reported regarding blood as a non-Newtonian fluid [12,13]. Hence, it would be of paramount importance to explore the impact of non-Newtonian and phasic flow properties on the hemodynamic profile of the human coronary arterial tree.

The aim of this study was to investigate the spatial and phasic WSS distribution during the cardiac cycle in a normal human left main coronary artery (LMCA) bifurcation computational model treating blood as a non-Newtonian fluid. At the same time, a pathogenetic link between WSS oscillations and atherogenesis was attempted.

Methods

Three-dimensional geometry

The 3D geometry of the LCA computational model used has been reported elsewhere on the basis of data compiled from several sources [9,14]. In particular, the investigated model included the LMCA and its two main branches, namely the left anterior descending (LAD) and the left circumflex (LCx) arteries (Fig. 1). The length and average diameters of our model were as follows: LMCA length, 11.0 mm; LMCA, LAD and LCx average diameters, 4.0, 3.4 and 3.0 mm, respectively. The centerline angles between LMCA and LAD, LMCA and LCx, and LAD and LCx were 159°, 117° and 84°, respectively. Finally, the LAD and LCx radii of curvature were constant with values of 42.8 and 39.3 mm, respectively.

Mesh generation

The 3D geometry data were incorporated in a preprocessing code (Gambit 2.0; Fluent Inc., Lebanon, NH, USA) for unstructured mesh generation (Fig. 1). This code, using the TGrid meshing algorithm, created a volume mesh that primarily consisted of 61.635 tetrahedral elements, corresponding to 14.147 nodes.

Fig. 1

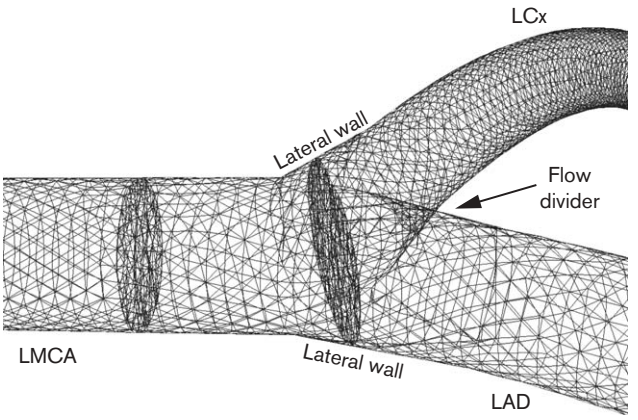

Three-dimensional geometry of the utilized left coronary artery bifurcation model along with the unstructured mesh on its luminal surface. LAD, left anterior descending; LCX, left circumflex; LMCA, left main coronary artery.

Boundary conditions

The blood flow was considered as 3D, unsteady and laminar, while the arterial walls were assumed to be inelastic and impermeable. The blood density ρ was assumed to be constant at 1058.0 kg/m^3, whereas blood was treated as a non-Newtonian fluid obeying the power law [15]. At the luminal surface, a no-slip boundary condition was applied such that velocity components parallel to the wall were zero. The Reynolds (*Re*) and Womersley (*Wo*) numbers that characterized the flow were set equal to 58 and 1.47, respectively. Furthermore, to investigate the influence of blood viscosity properties on the spatiotemporal behavior of the flow, the same phasic simulation was performed considering blood as a Newtonian fluid with a constant viscosity of 0.00345 kg/m-s.

Phasic flow

To simulate the physiological phasic flow conditions in LCA, a typical inlet flow velocity waveform was applied (Fig. 2). This waveform corresponds to the average physiological human left coronary flow and has been widely cited in the medical literature [2,16]. The cardiac cycle period was set equal to 1000 ms, of which 300 ms corresponded to systole and the remaining 700 ms to diastole; thus, their duration ratio was regarded as approximately 1 : 2 [16]. Two hundred solution time-steps were utilized to describe the velocity waveform and subsequently to elucidate the temporal variation of flow parameters. At the LMCA entrance, the velocity was

Fig. 2

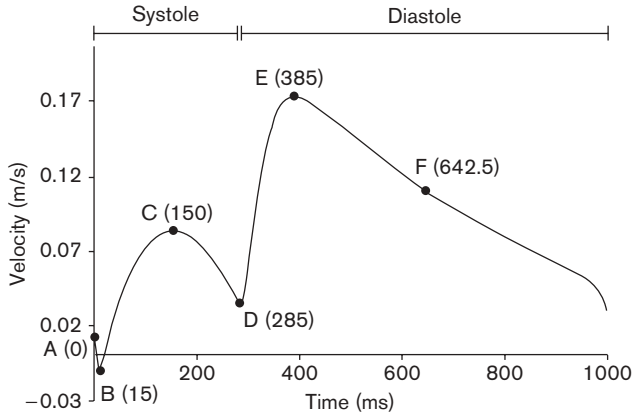

The normal blood velocity waveform in the left coronary artery.

considered to be uniform over the cross-section at each time step.

From the entire velocity waveform, six characteristic time-points, namely A, B, C, D, E and F, were selected (Fig. 2). In detail, point A refers to the start of the cardiac cycle, representing the start of isovolumetric contraction, while point B occurs 15 ms after the onset of systole corresponding to reversed flow (negative velocity). Point C occurs after 150 ms and corresponds to the peak of the ejection phase. Point D occurs 285 ms after the start of systole, simultaneously with the insicura of the aortic pressure waveform (closure of the aortic valve) representing the end of systole. Point E occurs 385 ms after point A, at the peak of diastole. Finally, point F, occurring 642 ms after the onset of systole, represents the mid-diastolic phase.

The applied initial flow conditions, referring to velocity and pressure distribution over the flow field, were computed from the entrance flow velocity during the first time-step of the phasic waveform. For computational purposes, the branching lengths were chosen to be long enough to satisfy uniform outlet flow conditions. These conditions required that the outlet fluxes in LAD and LCx were proportional to their cross-sectional areas; hence, the flow split ratio between LAD and LCx was set equal to 1.7.

Calculated variables

All mesh and flow data were transferred to the main CFD solver (Fluent 6.0; Fluent Inc, Lebanon, NH, USA). This numerical code solved the classical Navier–Stokes' flow equations for continuity and momentum [2].

The main calculated variable was the WSS (N/m^2) defined as the product of velocity gradient at the wall and blood viscosity [2]. The spatiotemporal distribution of WSS was investigated in two distinct regions of the LMCA bifurcation, namely the flow divider and the lateral walls, constituting the inner and outer walls of the bifurcation, respectively (Fig. 1). At these regions, the minimum WSS (minWSS), maximum WSS (maxWSS) and mean WSS (meanWSS) values were calculated for all time points. Moreover, to study the influence of flow pulsation on WSS variation [17], we calculated the variable ΔWSS defined as follows:

$$\Delta\mathrm{WSS_r} = \frac{\max \mathrm{WSS_r} - \min \mathrm{WSS_r}}{\max \mathrm{WSS_b}}, \qquad (1)$$

where $\mathrm{maxWSS_r}$ and $\mathrm{minWSS_r}$ were the maximum and minimum WSS values over the cardiac cycle at a given region 'r' on the arterial wall and $\mathrm{maxWSS_b}$ was the maximum WSS value over the entire bifurcation region.

Results

Qualitative analysis

Figure 3 shows the spatial distribution of WSS at the entire LMCA bifurcation region at all time points. It is notable that the WSS distribution was highly non-uniform owing to the complex 3D geometry of the LCA. In particular, WSS experienced higher values at the LMCA from its ostium up to few millimeters before the bifurcation throughout the entire cardiac cycle (yellow and green regions). At the bifurcation region, this parameter revealed lower values at the lateral walls (blue regions) and higher values at the flow divider. This 'ring-shaped' low WSS region at the bifurcation was evident during the entire cardiac cycle. Finally, the region, that was in contact with the myocardial surface exhibited low WSS as well, probably because of the inner curvature of the coronary artery, while distally to the bifurcation, the LAD and LCx regions experienced higher WSS values. Figure 4 depicts the spatial variation of WSS at points B (early systole) and E (peak diastole), revealing a significant WSS oscillation in both magnitude and direction at early systole.

Quantitative analysis

Figure 5 presents the variation of minWSS, maxWSS, meanWSS and ΔWSS values at the flow divider and lateral walls for all time points (from A to F). The WSS in the entire bifurcation region ranged from 0.085 to 5.97 N/m^2. The value of 5.97 N/m^2 was used in variable $\mathrm{maxWSS_b}$ of equation (1) for the calculation of ΔWSS. The flow divider region encountered higher meanWSS and minWSS values than the lateral walls for all time steps of the pulsatile waveform (Fig. 5a and c, respectively), whereas maxWSS showed almost equal values in both the flow divider and lateral wall regions during the cardiac cycle (Fig. 5d). ΔWSS revealed higher values in the lateral walls than in the flow divider (Fig. 5b).

Fig. 3

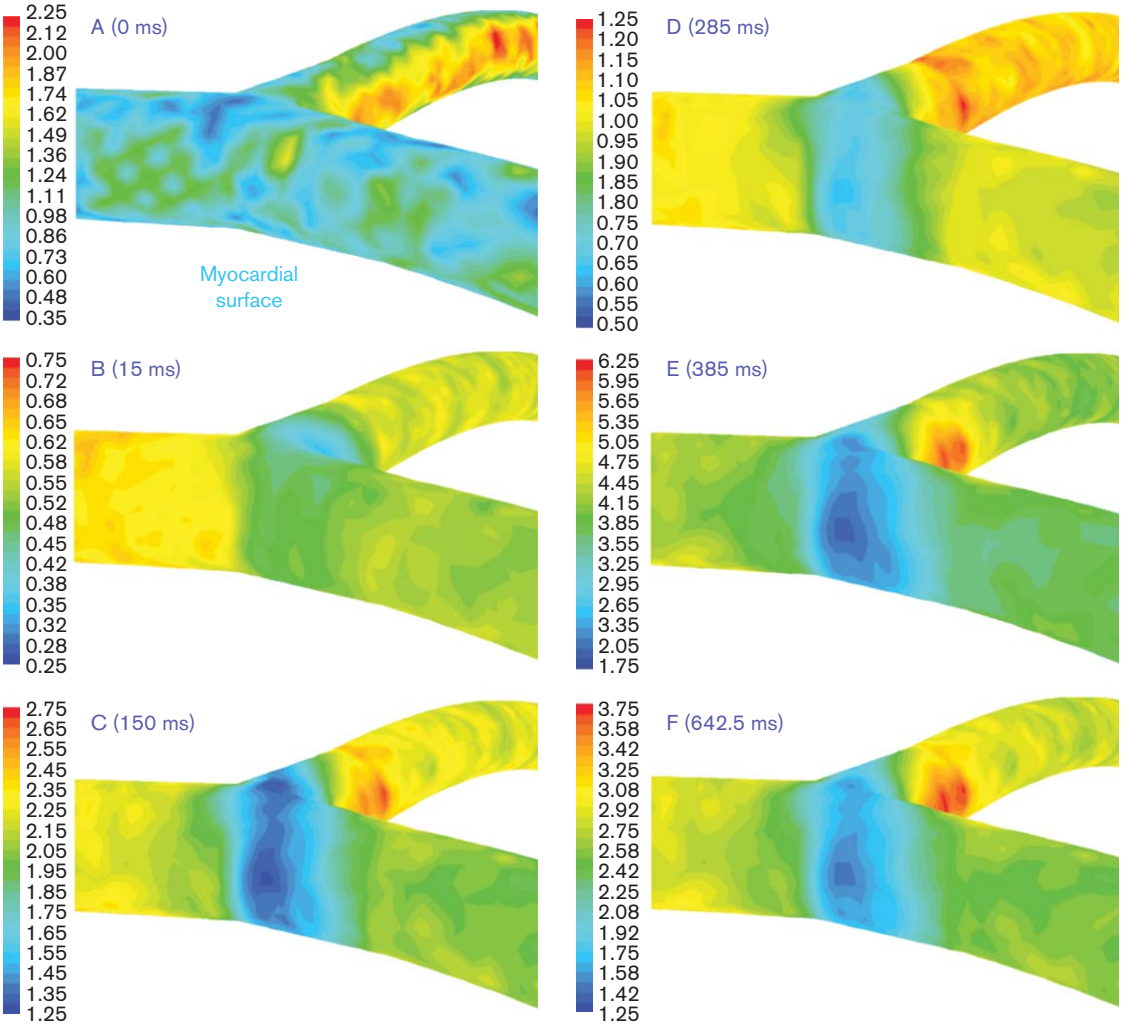

Spatial distribution of wall shear stress (WSS, N/m^2) at the entire bifurcation region for all time points (from A to F). Notice the 'ring-shaped' low WSS contour region at the bifurcation after 150 ms (point C).

As far as the temporal variation of WSS is concerned, all the variables (maxWSS, minWSS, meanWSS and ΔWSS) exhibited a similar pattern with higher values in diastole than in systole at both the flow divider and the lateral walls. In particular, at the lateral walls, the meanWSS increased from 1.64 N/m^2 at peak systole (point C) to 2.83 N/m^2 at peak diastole (point E), thus by almost 73%, while at the flow divider the meanWSS experienced a 108% increase (from 2.13 to 4.43 N/m^2).

With regard to the influence of blood properties on the spatiotemporal variation of WSS, it was found that, regardless of the non-Newtonian or Newtonian behavior, the meanWSS followed the aforementioned spatial and temporal patterns throughout the cardiac cycle (Fig. 6). The Newtonian WSS, however, experienced consistently lower values during the entire cardiac cycle than the non-Newtonian WSS.

Discussion

Spatial variation of wall shear stress and atherogenesis

The spatial distribution of WSS found in our study was in perfect agreement with other similar computational studies [1,4,9]. Additionally, using the variable ΔWSS as a measure of WSS oscillation attributed to phasic flow, we found that the lateral walls encountered greater WSS oscillations than the flow divider (Fig. 5b). The above findings, in conjunction with several clinical observations that atherosclerosis is mainly localized at the lateral walls of bifurcation, while it spares the flow divider [18–20], support a pathogenetic implication of low WSS on

Fig. 4

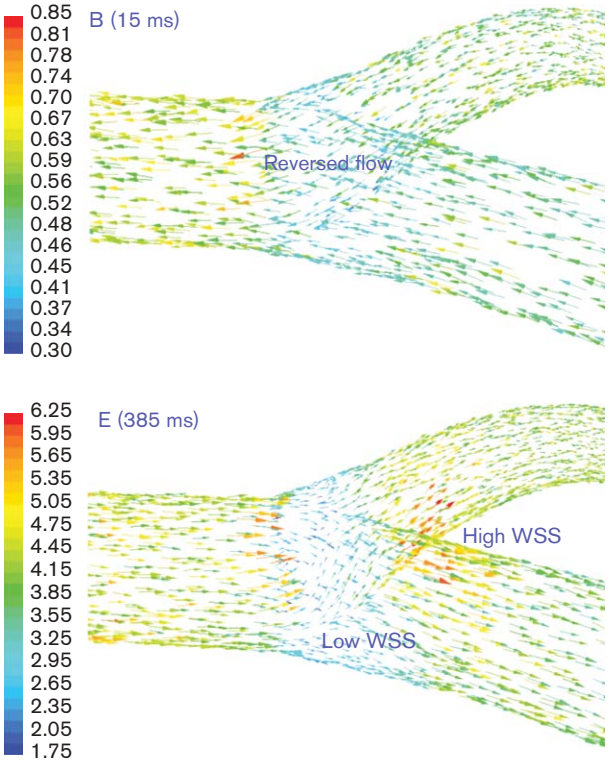

Vector distribution of wall shear stress (WSS, N/m^2) at time points B (early systole) and E (peak diastole), respectively. The length of the arrows is proportional to the WSS magnitude. The flow reversal both in magnitude and in direction at early systole (top) is evident. During diastole (bottom), the WSS experiences higher values at the flow divider (red arrows) and lower values at the lateral walls (blue arrows).

atherogenesis [5]. Moreover, this WSS distribution pattern in LMCA bifurcation was similar to the corresponding one found in the carotid bifurcation [10,18], suggesting that it could be extended to every bifurcation of the human arterial tree.

Phasic flow and atherogenesis

As mentioned, meanWSS revealed a significant temporal oscillation throughout the course of the cardiac cycle (Fig. 5a). This phasic pattern of WSS could be attributed to the physiological phenomena that occur during the cardiac cycle. In the course of systole, while the myocardium is ejecting the cardiac output, the epicardial coronary segments are filled with blood. As the intramyocardial segments of coronary arteries are almost collapsed during this phase of the cardiac cycle, because of the myocardial contraction, a retrograde blood flow is created and directed from the subendocardial to the epicardial coronary portions. As a result, this backward moving blood significantly reduces the flow in the large epicardial segments, eventually causing a substantial dilatation in them. As long as the WSS variation is proportional to the blood velocity variation, in the epicardial coronaries the WSS gradually increases up to its systolic maximum at mid-systole (point C) and then declines until the end of systole (point D). In diastole, as the blood starts to recirculate in intramyocardial coronary capillaries, the blood flow in the LCA markedly increases; thus, the WSS experiences a steeper increase until its diastolic maximum (point E). Eventually, the WSS slowly declines (point F) throughout the rest of the diastolic phase until the closure of the aortic valve and the initiation of the next systole. In other words, the WSS maintains significantly lower and oscillating values in systole than in diastole. Given the importance of low and oscillating WSS in atherogenesis, it seems reasonable to adopt the hypothesis that the systolic period favors the pathophysiological processes responsible for the onset and development of atherosclerosis (Fig. 7). In contrast, the steep increase in WSS, appearing in diastole, modulates a rather atheroprotective environment, compensating for the systolic atherogenic effect [4].

Apart from the low values during systole, the WSS experienced great temporal oscillations during the cardiac cycle ranging between the systolic minimum and the diastolic maximum. As presented in Fig. 4, a flow reversal was included in our model at the onset of systole (from point A to B), evoking a great WSS fluctuation in both magnitude and direction. Given the implication of oscillating WSS in atherogenesis [1,18], it could be postulated that not just the systolic phase by itself but also the cyclic WSS oscillation between systole and diastole favor atherogenesis (Fig. 7) [21]. Indeed, this atherogenic effect might be further intensified as these phasic WSS oscillations are gradually accumulated through life (‘concentrated stress effect’) [22].

The aforementioned cyclic hemodynamic phenomena could also imply an atheroprotective role of bradycardia or low heart rate [23,24]. According to clinical observations in humans and experimental animal studies, a high heart rate promotes atherosclerosis through different pathways including the sympathetic overactivity, the increased arterial wall stress and the reduced arterial compliance [25–27]. The possible direct effect of heart rate on WSS, however, has not been investigated yet. It could be hypothesized that as diastole lasts longer than systole (duration ratio of 2 : 1, approximately) in bradycardia or low heart rate, it compensates for the atherogenic low WSS values occurring during systole. In contrast, as the heart rate increases, an increase in the total time spent on systoles per minute relative to diastole occurs, because of shortening of diastolic time, while at the same time the number of the cardiac cycles per minute increase [16,21]. Thus, in regions susceptible to atherosclerosis, the atherogenic effect of high heart rate might be attributed to two potential mechanisms, namely the intensification of the exposure of the endothelium to the atherogenic

Fig. 5

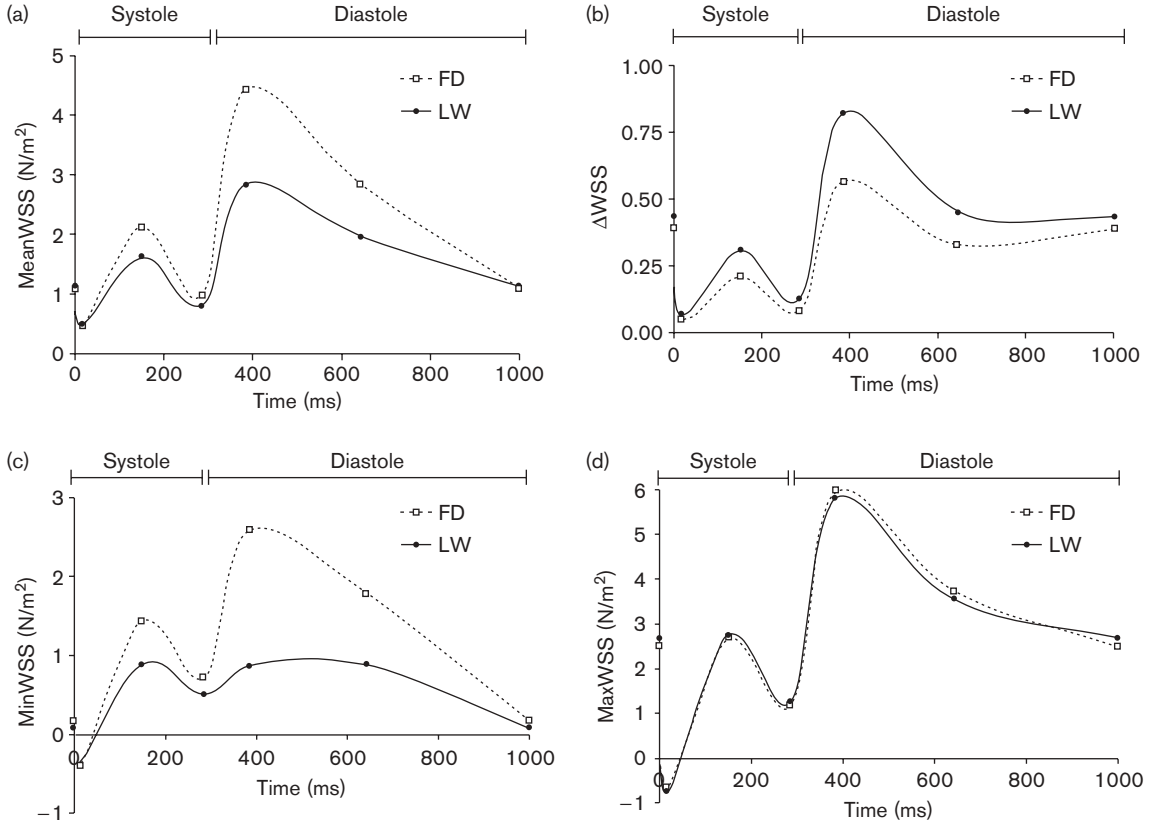

Temporal oscillation of (a) mean WSS (mean WSS), (b) Δ WSS at the flow divider (FD) and lateral walls (LWs) of the left main coronary artery bifurcation, (c) minimum wall shear stress (WSS) (min WSS) and (d) maximum WSS (Max WSS).

Fig. 6

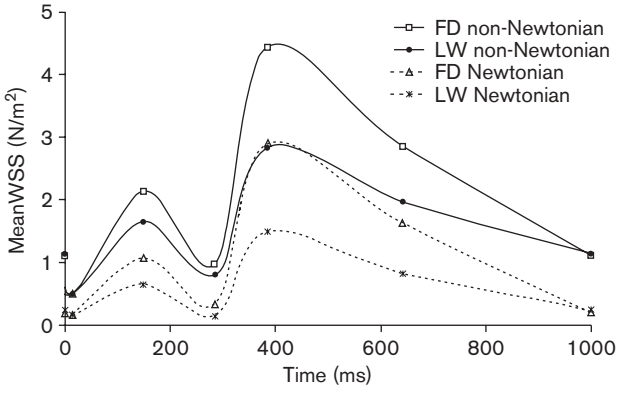

The spatiotemporal variation of mean wall shear stress (meanWSS) under non-Newtonian and Newtonian blood viscosity properties. Although the Newtonian WSS experienced consistently lower values throughout the entire cardiac cycle than the non-Newtonian WSS, the general pattern of lower WSS values at the lateral walls and during systole was evident regardless of the blood properties.

effects of low systolic WSS and the increase in the frequency of phasic WSS oscillations per minute. Both phenomena are very likely to be augmented over the long term (Fig. 7).

Pathogenetic linkage of low and oscillating wall shear stress with atherogenesis

Under resting conditions, the WSS forces constitute a critical modulator in maintaining normal physiologic endothelial function and morphology producing a significant atheroprotective effect [1,28]. The WSS, however, can potentially exert atherogenic effects in regions where the flow is disturbed. On the basis of laboratory findings, it seems that the low and oscillatory WSS interplays with the endothelial cells activating them through complex pathways [29,30]. In particular, membrane integrins, ion channels and G proteins have been recognized as mechanosensors, converting the WSS stimuli into biochemical signals. These signals in turn trigger downstream intracellular signalling pathways, which eventually increase the activity of specific tran-

Fig. 7

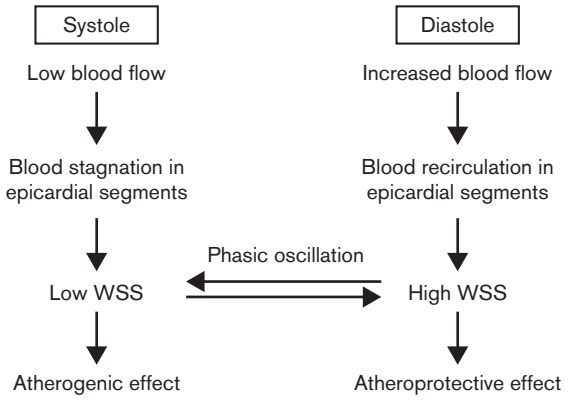

Proposed mechanisms for the atherogenic effect of phasic flow: the low blood flow in epicardial coronary segments during systole may exert an atherogenic effect on the endothelium by modulating a low wall shear stress (WSS) environment. This effect is counterbalanced in the diastolic phase when the blood flow is accelerated. Additionally, this atherogenic action is further augmented by the WSS oscillations from the low systolic to the high diastolic values during the evolution of the cardiac cycle. Over the long term, these phenomena are gradually accumulated.

scription factors. Binding of these factors to DNA activates numerous atherogenic genes that regulate cell morphology, proliferation, apoptosis, differentiation, migration and secretion of prothrombotic and proinflammatory molecules. Moreover, these gene alterations affect the cytoskeletal fibers causing structural changes of the endothelial cells [31]. As a result, the cells become more permeable to the circulating lipoproteins and other circulating inflammatory substances [4,21,29]. This phenomenon is further augmented by the blood stagnation that occurs in low flow regions. In these regions, the residence time of blood atherogenic particles is increased, thus facilitating their subendothelial migration through the damaged endothelium [4,21].

Phasic versus steady flow

In this study, we applied a phasic flow to investigate the variation of WSS in space and time in a normal LMCA bifurcation. As mentioned, this approach was more realistic because the blood flow is pulsatile by its nature [32]. We found that the WSS exhibited lower values at the lateral walls than at the flow divider, a pattern that was evident throughout the entire cardiac cycle. In fact, the same pattern has also been revealed in several other studies in which the flow had been considered as steady [5]. Thus, it seems that the assumption of steady flow is adequate for studies focused on the spatial variation of the local hemodynamic variables; however, the major flaw in this approach is that it does not provide any information about the phasic oscillation of WSS, which according to our results seems to be a key modulator of the local atherogenic environment.

Newtonian versus non-Newtonian model

Although blood does not by nature exhibit a constant viscosity at all the flow rates – thus behaving as a non-Newtonian fluid [12] – for reasons of simplicity the great majority of the studies reported have considered circulating blood as Newtonian. While this simpler assumption in large arteries is widely accepted [33], questions remain unanswered about the viscosity of blood flow in the coronaries. In this study, we treated the blood as a non-Newtonian fluid obeying the power law. Moreover, we investigated the effect of Newtonian blood properties on the spatiotemporal behavior of the flow. We found that the Newtonian WSS experienced consistently lower values throughout the entire cardiac cycle than the non-Newtonian WSS; however, the general pattern of lower WSS values at the lateral walls, particularly during systole, was evident regardless of the applied blood properties. In addition, the non-Newtonian WSS distribution found in our computational model did not reveal any remarkable differences as compared with other similar studies, in which the Newtonian model was utilized [2,9]. It seems that when using CFD to investigate the WSS behavior, although less accurate, the simpler and more applicable assumption of Newtonian model will suffice [12]. Nevertheless, more analytical studies focused exclusively on this field are needed.

Limitations

Several limitations were noted in this study. First, the required time for the CFD simulation was long enough, limiting the on-site application of the method. It is anticipated, however, that the application of modern more powerful desktop computers will significantly eliminate this time. Second, although the 3D geometry used was representative of the normal human LCA bifurcation, it would be a great simplification to accept it as a generalized human in-vivo model. As there are many geometrical variations among humans, it would be more realistic to conduct a similar study on patient-based realistic 3D geometries. In future work, a larger representative dataset, including in-vivo time-varying 3D geometries derived by integration of intravascular ultrasound and biplane coronary angiography data, will be utilized, applying pulsatile flow based on personalized initial and boundary conditions.

Conclusions

We simulated the flow in a human normal bifurcation model separated into two distinct flow regions, namely the flow divider and the lateral walls, at which a detailed non-Newtonian phasic flow analysis was performed. The CFD analysis provided local details of WSS that could not be revealed directly from imaging, enabling a better understanding of the role of hemodynamics in plaque development and progression. We found that during the entire cardiac cycle the flow divider was subjected to relatively high WSS, while the regions opposite to the

flow divider, at the lateral walls, and the epicardial curvature of the bifurcation exhibited lower WSS. With regard to temporal variation, the WSS encountered lower values throughout systole than in diastole, suggesting a possible atherogenic effect of both the systolic phase by itself and the phasic oscillation of WSS from systole to diastole. The computational model used could constitute a generalized model for further phasic flow analyses and their possible implication in atherogenesis.

References

1 Feldman CL, Stone PH. Intravascular hemodynamic factors responsible for progression of coronary atherosclerosis and development of vulnerable plaque. *Curr Opin Cardiol* 2000; **15**:430–440.

2 Nosovitsky VA, Ilegbusi OJ, Jiang J, Stone PH, Feldman CL. Effects of curvature and stenosis-like narrowing on wall shear stress in a coronary artery model with phasic flow. *Comput Biomed Res* 1997; **30**:61–82.

3 Asakura T, Karino T. Flow patterns and spatial distribution of atherosclerotic lesions in human coronary arteries. *Circ Res* 1990; **66**:1045–1066.

4 Giannoglou GD, Soulis JV, Farmakis TM, Farmakis DM, Louridas GE. Haemodynamic factors and the important role of local low static pressure in coronary wall thickening. *Int J Cardiol* 2002; **86**:27–40.

5 Ku DN, Giddens DP, Zarins CK, Glagov S. Pulsatile flow and atherosclerosis in the human carotid bifurcation. Positive correlation between plaque location and low oscillating shear stress. *Arteriosclerosis* 1985; **5**: 293–302.

6 Zeng D, Ding Z, Friedman MH, Ethier CR. Effects of cardiac motion on right coronary artery hemodynamics. *Ann Biomed Eng* 2003; **31**: 420–429.

7 Zendehbudi GR, Moayeri MS. Comparison of physiological and simple pulsatile flows through stenosed arteries. *J Biomech* 1999; **32**:959–965.

8 Tu C, Deville M, Dheur L, Vanderschuren L. Finite element simulation of pulsatile flow through arterial stenosis. *J Biomech* 1992; **25**:1141–1152.

9 He X, Ku DN. Pulsatile flow in the human left coronary artery bifurcation: average conditions. *J Biomech Eng* 1996; **118**:74–82.

10 Perktold K, Peter RO, Resch M, Langs G. Pulsatile non-Newtonian blood flow in three-dimensional carotid bifurcation models: a numerical study of flow phenomena under different bifurcation angles. *J Biomed Eng* 1991; **13**:507–515.

11 Rindt CC, Steenhoven AA. Unsteady flow in a rigid 3D model of the carotid artery bifurcation. *J Biomech Eng* 1996; **118**:90–96.

12 Gijsen FJ, Allanic E, van de Vosse FN, Janssen GD. The influence of the non-Newtonian properties of blood on the flow in large arteries: unsteady flow in a 90 degrees curved tube. *J Biomech* 1999; **32**:705–713.

13 Farmakis TM, Soulis JV, Giannoglou GD, Zioupos GJ, Louridas GE. Wall shear stress gradient topography in the normal left coronary arterial tree: possible implications for atherogenesis. *Curr Med Res Opin* 2004; **20**: 587–596.

14 Nerem RM. Vascular fluid mechanics, the arterial wall and atherosclerosis. *J Biomech Eng* 1992; **114**:274–282.

15 Siauw WL, Ng EYL, Mazumdar J. Unsteady stenosis flow prediction: a comparative study of non-Newtonian models with operator splitting scheme. *Med Eng Phys* 2000; **22**:265–277.

16 Berne R, Levy M. *Cardiovascular physiology*. 8th ed. St Louis: Mosby; 2001.

17 Zeng D, Ding Z, Friedman MH, Ethier CR. Effects of cardiac motion on right coronary artery hemodynamics. *Ann Biomed Eng* 2003; **31**:420–429.

18 Giddens DP, Zarins CK, Glagov S. The role of fluid mechanics in the localization and detection of atherosclerosis. *J Biomech Eng* 1993; **115**:588–594.

19 Kuban BD, Friedman MH. The effect of pulsatile frequency on wall shear in a compliant cast of a human aortic bifurcation. *J Biomech Eng* 1995; **117**:219–223.

20 Fox B, James K, Morgan B, Seed A. Distribution of fatty fibrous plaques in young human coronary arteries. *Atherosclerosis* 1982; **41**:337–347.

21 Bassiouny HS, Zarins CK, Kadowaki MH, Glagov S. Hemodynamic stress and experimental aortoiliac atherosclerosis. *J Vasc Surg* 1994; **19**: 426–434.

22 Thubrikar MJ, Robicsek F. Pressure-induced arterial wall stress and atherosclerosis. *Ann Thorac Surg* 1995; **59**:1594–1603.

23 Palatini P. Heart rate: a strong predictor of mortality in subjects with coronary artery disease. *Eur Heart J* 2005; **26**:943–945.

24 Diaz A, Bourassa MG, Guertin MC, Tardif JC. Long-term prognostic value of resting heart rate in patients with suspected or proven coronary artery disease. *Eur Heart J* 2005; **26**:967–974.

25 Skantze HB, Kaplan J, Pettersson K, Manuck S, Blomqvist N, Kyes R, *et al*. Psychosocial stress causes endothelial injury in cynomolgus monkeys via beta1-adrenoceptor activation. *Atherosclerosis* 1998; **136**:153–161.

26 Palatini P. Heart rate as a risk factor for atherosclerosis and cardiovascular mortality: the effect of antihypertensive drugs. *Drugs* 1999; **57**:713–724.

27 Palatini P, Julius S. Heart rate and the cardiovascular risk. *J Hypertens* 1997; **15**:3-17.

28 Malek AM, Alper SL, Izumo S. Hemodynamic shear stress and its role in atherosclerosis. *JAMA* 1999; **282**:2035–2042.

29 Cunningham KS, Gotlieb AI. The role of shear stress in the pathogenesis of atherosclerosis. *Lab Invest* 2005; **85**:9–23.

30 Lehoux S, Tedgui A. Signal transduction of mechanical stresses in the vascular wall. *Hypertension* 1998; **32**:338–345.

31 Barbee KA, Macarak EJ, Thibault LE. Strain measurements in cultured vascular smooth muscle cells subjected to mechanical deformation. *Ann Biomed Eng* 1994; **22**:14–22.

32 Ziegler T, Bouzourene K, Harrison VJ, Brunner HR, Hayoz D. Influence of oscillatory and unidirectional flow environments on the expression of endothelin and nitric oxide synthase in cultured endothelial cells. *Arterioscler Thromb Vasc Biol* 1998; **18**:686–692.

33 Wootton DM, Ku DN. Fluid mechanics of vascular systems, diseases, and thrombosis. *Annu Rev Biomed Eng* 1999; **1**:299–329.